# Degradation and Drug-Release Studies of a Poly(glycolide-*co*-trimethylene carbonate) Copolymer (Maxon)

**K. Noorsal,[1] M. D. Mantle,[2] L. F. Gladden,[2] R. E. Cameron[1]**

[1]*Cambridge Centre for Medical Materials, Department of Materials Science and Metallurgy, University of Cambridge, New Museums Site, Pembroke Street, Cambridge CB2 3QZ, United Kingdom*

[2]*Department of Chemical Engineering, University of Cambridge, New Museums Site, Pembroke Street, Cambridge CB2 3RA, United Kingdom*

Received 5 February 2004; accepted 24 May 2004
DOI 10.1002/app.21108
Published online in Wiley InterScience (www.interscience.wiley.com).

**ABSTRACT:** Poly(glycolide-*co*-trimethylene carbonate) is available commercially as a monofilament suture known as Maxon. The literature has shown that Maxon sutures possess a slow degradation rate of about 7 months and exhibit relatively high mechanical strength in comparison with other absorbable sutures. However, very few articles are available on the degradation of unoriented Maxon. This study was designed to explore the chemical and physical aspects of the degradation of unoriented Maxon and its potential as a drug-release device. Several analytical techniques were used, including mass measurements, simultaneous small-angle X-ray scattering and wide-angle X-ray scattering, and thermoporometry. Magnetic resonance imaging and drug-release measurements were carried out with UV spectroscopy. The results suggest that unoriented suture-based Maxon undergoes multiple stages of hydrolytic degradation, which involve hydration, and active and postactive periods. The drug-release mechanism is controlled by diffusion in the early degradation stages and polymer erosion in the later stages of release. © 2004 Wiley Periodicals, Inc. J Appl Polym Sci 95: 475–486, 2005

**Key words:** biodegradable; degradation; drug delivery systems

## INTRODUCTION

Most biodegradable polymers are designed to degrade through hydrolysis. This is advantageous when they are used as media for controlled drug delivery as it eliminates the need for removing the delivery device after the release of the active agent has been completed. The use of poly(glycolide-*co*-trimethylene carbonate) as absorbable sutures is widely known, and there is a considerable body of literature on the degradation of the sutures.[1–4] The material is claimed to have better flexibility than pure polyglycolide (PGA) and achieves its total absorption in approximately 7 months.[4] However, little consideration has been given to the degradation behavior of unoriented poly(glycolide-*co*-trimethylene carbonate), and its potential as a drug-delivery device has not been fully exploited.

Poly(glycolide-*co*-trimethylene carbonate) is a triblock (ABA) copolymer also known as polyglyconate. Two forms are available, Maxon B and suture-based Maxon. Typically, it consists of PGA and poly(trimethylene carbonate) (PTMC) with a weight ratio of 67:33.[5,6] Suture-based Maxon, which is the subject of this article, is made of a random copolymer of PGA and PTMC in the middle block (B), whereas PGA forms the end blocks of the copolymer (A). This formulation differs from that of Maxon B, in which the middle block (B) is purely PTMC, whereas PGA forms the end blocks (A).

Previous work on PGA in our laboratory has led to the proposition of four-stage hydrolytic bulk erosion degradation involving reaction–erosion fronts.[7–9] Significant polymer erosion only starts at the beginning of stage 3 (after about 7 days), and during this stage, the polymer depolymerizes to a critical molecular weight that allows shorter chain polymer to diffuse into the surrounding medium. This hypothesis suggests that the reaction–erosion fronts move from the surface to the interior of the polymer. The drug is thought to be released from the hydrated regions behind the fronts, and release is complete when the fronts meet in the center. The reaction–erosion fronts move at the same rate through PGA samples of different sizes. At a given time, thicker samples therefore possess greater amounts of unswelled material ahead of the reaction–erosion fronts, and full release takes longer to complete. Based on this four-stage hydrolytic degradation, this article examines the degradation and drug-release properties of unoriented suture-

*Correspondence to:* R. E. Cameron (rec11@cus.cam.ac.uk).
Contract grant sponsor: Sirim Berhad (Malaysia).
Contract grant sponsor: Cambridge Commonwealth Trust.

based Maxon and compares these processes with those of the unoriented homopolymer PGA. The effect of the sample thickness on the degradation and how it controls the drug-release behavior of the polymer are investigated. The drug-release studies in this work primarily used theophylline as the model drug, and a comparison was made with a second model drug, sulfadiazine.

## EXPERIMENTAL

### Sample preparation

Disc-shaped suture-based Maxon samples were prepared with clear 2-0 Maxon sutures (Davis and Geck, Danbury, CT) 0.375 mm in diameter and 65 cm long. The sutures were first cut and crushed into small pieces in a mortar before being placed into an aluminum mold on a hot press. For drug-loaded samples, the crushed sutures were mixed with 5 wt % powdered theophylline or sulfadiazine (Sigma–Aldrich), which was used as the model drug, before being melt-compressed. The mold produced discs 0.3–2 mm thick with a diameter of 8 mm. During disc formation, the filled mold was compressed for about 1 min at a pressure of 10 bar at 240°C. The melted polymer was then immediately quenched in iced water. The top and bottom of the mold were covered with a 0.05-mm-thick Kapton HN (polyamide) film (Goodfellows, Cambridge, England) to ensure the ease of removal of the mold from the hot press and good thermal contact between the polymer and the iced water during the quenching. The melt-compression process produced good quenched and transparent suture-based Maxon samples with approximate weights of 27 (from the 0.3-mm-thick mold) to 130 mg (from the 2.0-mm-thick mold).

### Degradation and drug release

The degradation and drug release of the suture-based Maxon samples were carried out in a 0.01*M* phosphate-buffered saline (PBS) solution of pH 7.4 at 37 ± 0.5°C for predetermined times. The PBS solutions were prepared from PBS tablets (Sigma, Gillingham, Dorset, UK). Samples containing sulfadiazine were degraded in 0.3*M* PBS because sulfadiazine has a lower solubility in 0.01*M* PBS and is readily soluble in 0.3*M* PBS. The buffer solution and all the apparatus used in this study were autoclaved at 120°C with a pressure of 1 bar before use. The concentrated buffer (0.3*M*) was not autoclaved in this work as autoclaving the solution led to the precipitation of the buffer salts. Generally, a 20-mg sample with a 20-mL buffer solution was used for degradation. For the drug-release measurements, samples were placed in 100-mL PBS solutions with a copper wire, without agitation. The drug-release medium was withdrawn periodically for analysis and was returned back to its container for further accumulative measurements. The degradation and drug-release specimen bottles were shaken regularly by hand. The drug concentrations were measured with a Uvikon 931 UV spectrometer (Germany) with the following UV values: at 0.01*M* PBS, the maximum wavelength ($\lambda_{max}$) was 271 nm (±7%) and the molar extinction coefficient ($\varepsilon$) was 563.4 $mg^{-1}$ $cm^2$ for theophylline, and at 0.3*M* PBS, $\lambda_{max}$ was 240 nm (±7%) and $\varepsilon$ was 696 $mg^{-1}$ $cm^2$ for sulfadiazine.

### Changes in the mass and pH

The measurements of the water uptake and mass loss of the polymer during degradation were made with a microbalance to an accuracy of ±0.1 mg. The water uptake was calculated by the subtraction of the dry mass from the wet mass of the degraded samples, whereas the mass loss was calculated as the difference in the masses of the dry degraded sample and the undegraded samples. Upon the completion of the degradation, the samples were removed from their degradation solution, dabbed dry, and weighed immediately to minimize error caused by water evaporation. The samples were then dried for 3 days at 50°C in a vacuum oven at a pressure of 800 mbar. The dry weight was then obtained. Both the water uptake ($M_{gain}$) and mass loss ($M_{loss}$) were expressed as percentages:

$$M_{gain} = \left(\frac{M_w - M_d}{M_0}\right) \times 100 \quad (1)$$

$$M_{loss} = \left(\frac{M_d - M_0}{M_0}\right) \times 100 \quad (2)$$

where $M_w$ is the wet mass, $M_d$ is the dry mass, and $M_0$ is the initial dry mass of the sample.

### Magnetic resonance imaging (MRI)

MRI was used to monitor water ingress into the polymer during degradation, and pulsed field gradient (PFG) nuclear magnetic resonance (NMR) was used to determine the self-diffusion coefficient of water ($D$) residing within the polymer matrix. The basic principles of NMR and MRI can be found in standard texts.[10,11] The experimental procedure used in this work closely followed that of Milroy et al.[9] to allow a comparison to be made between the MRI data of pure PGA discs and suture-based Maxon discs used in this study.

Spatially resolved MRI images were obtained with a slice-selective two-dimensional $^1H$ spin-density imaging protocol to record the water ingress into suture-

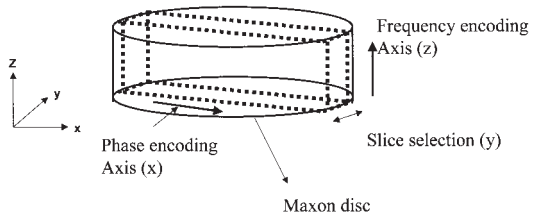


**Figure 1** Schematic diagram showing the location of the slice selected from the *x*–*z* plane in a suture-based Maxon disc to record two-dimensional MRI data. (Reprinted with permission from G. E. Milroy et al. (2003). Copyright 2003 J Mater Sci: Mater Med.)

based Maxon discs in the *x*–*z* plane with a spin-echo pulse sequence technique (see Fig. 1). All the experiments were conducted with a Bruker DMX 300 NMR spectrometer (Germany) operating at a proton resonance frequency of 300.13 MHz. Suture-based Maxon samples 2 mm thick and 8 mm in diameter were placed on a Perspex support inside a specially made Perspex tube and then were placed in the MRI spectrometer. Each MRI image that was recorded corresponded to a different polymer sample. To minimize water evaporation, all the samples were wrapped in cling film before the imaging. A microimaging probe head equipped with a 15-mm $^1$H birdcage radio-frequency coil was used to obtain $^1$H images of 64 pixels $\times$ 128 pixels in a field of view of 10.0 mm $\times$ 0.5 mm; the in-plane spatial resolution was 156 $\mu$m $\times$ 39 $\mu$m in the *x* and *z* directions, respectively. The spatial resolution was obtained with shielded magnetic field gradients of 94.7 and 35.61 G/cm in the $G_z$ and $G_x$ directions and of 5.42 G/cm for the $G_y$ slice gradient. The *x*–*z* slice thickness was 1.5 mm. A data-acquisition time of approximately 28 min was used to achieve an acceptable signal-to-noise ratio. The minimum echo time was 2.52 ms, and the repetition time was chosen to be at least 3 times greater than the spin–lattice relaxation time of the sample under study.

In addition to the standard spin-echo imaging sequence, this work used the PFG NMR technique to measure *D*, as first described by Stejskal and Tanner.[12] The relationship between the $^1$H-NMR signal intensity and *D* is given by

$$S(g)/S(0) = \exp[\,-\gamma^2\delta^2\mathrm{ginc}^2 D(\Delta - \delta/3) \qquad (3)$$

where $S(g)$ is the observed $^1$H signal, ginc is the PFG increment, $S(0)$ is the signal strength when the gradient pulse strength (ginc) equals zero, $\gamma$ is the gyromagnetic ratio of the nucleus under observation, $\Delta$ is the gradient pulse spacing, and $\delta$ is the length of time that the gradient is applied in the experiment. *D* is determined from the gradient of a plot of the natural logarithm of the signal intensity ratio $S(g)/S(0)$ (or simply *S*) versus $\gamma^2\mathrm{ginc}^2(\Delta - \delta/3)$. For free diffusion, that is, Brownian diffusion, the plot gives a straight line with a slope equal to $-D$ ($m^2/s$). Table I shows the PFG experimental acquisition parameters used in this work.

### Simultaneous small-angle X-ray scattering (SAXS) and wide-angle X-ray scattering (WAXS)

Simultaneous SAXS and WAXS measurements of the wet degraded samples were taken on Station 8.2 of the Daresbury Synchroton Radiation Source. The SAXS data were collected on a quadrant detector upon a 12-s exposure of 25 frames and then were normalized with an ionization chamber placed after the sample. This was to correct for fluctuations in the beam intensity and sample thickness. The intensity was also divided by the response of the detector to a uniform radiation from a $^{55}$Fe source. In addition, the intensity was also corrected by the subtraction of the background signal from an empty signal holder. Finally, the SAXS data were calibrated with the positions of known peaks of wet rat-tail collagen. The WAXS data were collected on a curved INEL detector (France), which covered $2\theta = 120°$ at a radius of 0.2 m. The WAXS data were calibrated to $2\theta$ with a high-density polyethylene sample.

The Lorentz correction was applied to correct the scattering data to those from a single lamellar stack. The long period (*d*; i.e., the repeat distance of stacks of lamellar crystals) was calculated from the peak position of the Lorentz-corrected data with the Bragg equation [eq. (4)]. The invariant (*Q*) or scattering power depended on the electron density between the crystalline and amorphous phases and the volume fractions and was calculated with eq. (5):

$$d = \frac{2\pi}{q_{\max}} \qquad (4)$$

$$Q = \int_0^\infty \mathbf{q}^2 I(\mathbf{q})\, d\mathbf{q} \qquad (5)$$

where $q_{\max}$ is the location of the peak maximum, $\mathbf{q}$ is the scattering vector, and $I(\mathbf{q})$ is the intensity at $\mathbf{q}$. *Q* was assessed with Simpson's rule, with which the

**TABLE I**
**Experimental Acquisition Parameters Used for PGSTE**

| Parameter | Units | Acquisition |
|---|---|---|
| $\delta$ | ms | 3 |
| $\Delta$ | ms | 100 |
| $\gamma$ | $\mathrm{rads}^{-1}/\mathrm{T}^{-1}$ | $2.675 \times 10^8$ |
| ginc | T/m | 0.05–0.8 in 10 steps |

integration of the area under an $I(\mathbf{q})\mathbf{q}$–$\mathbf{q}$ plot can be calculated.[13]

### Thermoporometry

Thermoporometry can be used in measuring the pore size distribution in the range of 2–50 nm.[14] This technique allows the measurement of the pore structures in a wet environment, which represents the natural state of the degrading polymer. A detailed theoretical discussion of thermoporometry was published by Brun et al.,[15] in which the basic principle was reported (1) to lie in the depression of the freezing or melting point of a material because of the strong curvature of the solid–liquid interface present within the small pores and (2) to be detected calorimetrically.

The size of confined ice crystals is inversely proportional to the degree of undercooling [$\Delta T = T_f - T_0$, where $T_0$ is the normal phase transition of a liquid (0°C for water) and $T_f$ is the temperature at which the phase transition is actually observed].

Equations (6)–(8) were used in measuring the pore size distribution, as water was used as the hydrolysis medium, under the assumption that it was a cylindrical-pore-shape material.

The pore radius [$R_p$ (nm)] and the apparent heat of fusion [$\Delta H_a(T)$], which was temperature-dependent, were obtained as follows:

$$R_p = A - \frac{B}{\Delta T} \tag{6}$$

$$\Delta H_a(T) = \Delta H_f + C\Delta T + D(\Delta T)^2 \tag{7}$$

where $\Delta T$ is the melting point depression and $\Delta H_f$ is the heat of fusion of water under normal conditions (332 J/g). The values for the constants were $A = 0.68$ nm, $B = 32.33$ nm K, $C = 11.39$ J g$^{-1}$ K$^{-1}$, and $D = 0.155$ J g$^{-1}$ K$^{-1}$ for heating in cylindrical pores.[14]

The pore volume with radii between $R_p$ and $R_p + dR_p$ was calculated with eq. (7), in which $\Delta H_a(T)$ is expressed in J/g. The pore volume distributions may be represented as $dV/dR_p$ as a function of $R_p$:

$$\frac{dV}{dR_p} = \frac{k(\Delta T)^2(dq/dt)}{\Delta H_a(T)} \tag{8}$$

The quantity $dV/dR_p$ is given as the amount of the pore volume (per gram of dry material) measured in a certain pore size interval divided by the size of that interval.

Data were collected with a PerkinElmer DSC7 (Wellesley, MA). Degraded samples of suture-based Maxon 1.5 mm thick and 8.0 mm in diameter were used in this study. The samples were dabbed dry with clean tissue to remove the surface water. The samples (ca. 25 ± 0.001 mg) were crimped shut in the sample pans. The temperature was dropped rapidly to −50°C at a rate of 200°C/min and then held there for 5 min to freeze the water. The samples were then heated at a rate of 10°C/min to 10°C. The heat-flow measurements were made against an empty pan as a reference.

### Gel permeation chromatography (GPC)

The variation in the sample molecular weight upon degradation was determined with GPC. The GPC experiments were very kindly performed by Smith and Nephew, Ltd. (York, England). Both suture-based Maxon samples, undegraded (before significant degradation) and degraded for 35 days (after significant degradation), were first dried in a vacuum oven before being crushed with a steel pestle and mortar. The samples were stored in a desiccant before being dispatched and then were dissolved in hexafluoroisopropanol for analysis.

## RESULTS

### Changes in the physical appearance

Undegraded suture-based Maxon samples appeared to be light brown and transparent. During degradation, the polymer gradually became opaque, and cracks appeared. The samples were partially opaque after 10 days and became fully opaque after 30 days. Thicker samples seemed to become opaque more quickly than the thinner ones. After 30 days, cracks were visible and became larger after longer degradation times.

### Changes in the mass and pH

Figure 2 shows the water uptake and mass loss of suture-based Maxon samples as a function of the degradation time. Very little water uptake and mass loss was seen over the first 20 days in any of the samples. The mass loss and water uptake started to increase slowly after 20 days and more quickly after 40 days. Incorporating theophylline into 2.0-mm-thick samples may have produced a slightly greater rate of water uptake and mass loss, an effect that was not apparent in the thinner samples with 0.3 or 1.0 mm thick (not shown). Both the water uptake and mass loss were largely unaffected by the sample thickness, although it is possible that the onset was slightly later in the thicker samples.

Figure 3 shows the pH of the buffer solution as a function of the degradation time. The timescale of the behavior mirrored that of the mass loss, the pH falling as a result of the release of acidic degradation products.

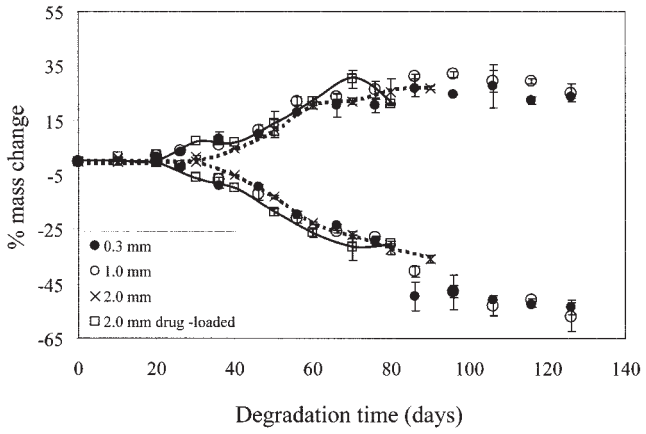


**Figure 2** Changes in the water and mass loss of suture-based Maxon with the degradation time, showing the effects of theophylline incorporation into the samples and sample thickness. For clarity, the 2-mm-thick suture-based Maxon samples, blank and drug-loaded, are represented by dotted and solid lines, respectively.

## MRI

Figure 4(a) shows two-dimensional slice-selective MRI images of blank suture-based Maxon degraded in unstirred solutions at various time points. No water signal could be obtained for samples degraded for less than 30 days. Between 35 and 50 days, a very weak water signal (appearing dark gray in the images) could be observed throughout the sample, which agreed well with the low level of water uptake presented in Figure 2. A sharp increase in the water uptake (up to 20 wt %) was observed between 50 and 60 days. Between days 60 and 80, a moderate increase in the overall water uptake could be observed, and water was more evenly distributed throughout the samples.

Figure 4(b) examines the effect of stirring during degradation. No obvious effect could be seen for samples degraded between 35 and 40 days. However, after 50 days, the stirred samples seemed to exhibit a higher overall water signal, especially at the edges. By 60 days, the water distribution was homogeneous. Figure 4(c) illustrates the effect of the presence of theophylline on the uptake of PBS within unstirred samples and shows a slightly higher uptake of water than that for the unstirred samples of only Maxon [Fig. 4(a)]; this is supported by the data given in Figure 2. The effect of stirring the solutions of the drug-loaded samples was quite apparent in the samples degraded for 50 days [Fig. 4(d)], for which the water signal was significantly higher throughout the samples.

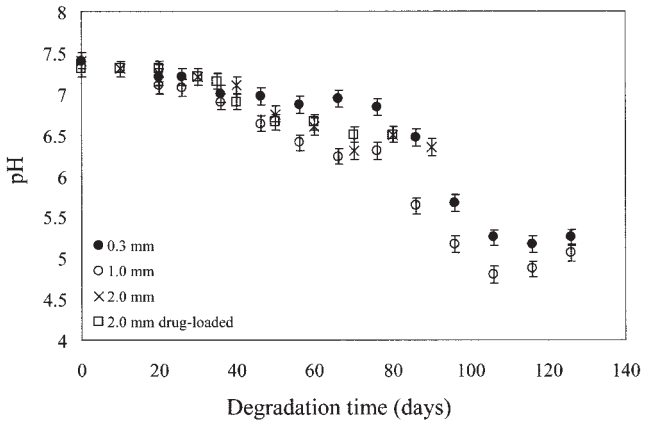


**Figure 3** Changes in the pH of the degradation medium with the degradation time. The effects of the sample thickness and the incorporation of theophylline are also shown.

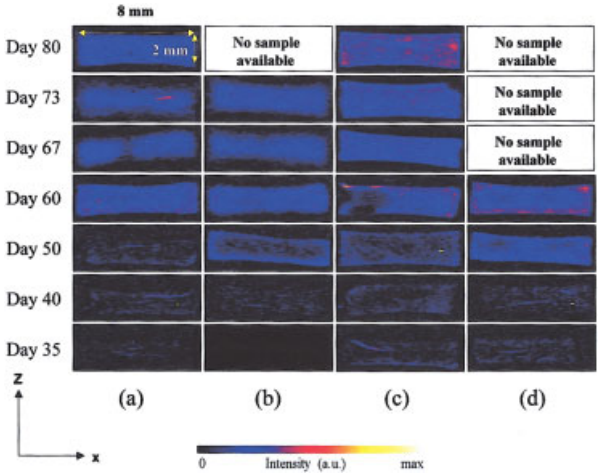


**Figure 4** $^1$H MRI images of (a) blank suture-based Maxon degraded in an unstirred solution, (b) blank suture-based Maxon degraded in a stirred solution, (c) drug-loaded suture-based Maxon degraded in an unstirred solution, and (d) drug-loaded suture-based Maxon degraded in a stirred solution. The cross sections of the Maxon discs were 2 mm thick and 8 mm in diameter. Water appears as light blue and pink. [Color figure can be viewed in the online issue, which is available at www.interscience.wiley.com.]

Blank suture-based Maxon samples were also degraded for 136 days in 100% $D_2O$. The aim was to determine whether the polymer mobilized sufficiently during degradation to give a $^1$H MRI signal. No signal was observed. This confirmed that the signal from the sample degraded in $H_2O$ was from water alone.

Table II shows the diffusion coefficients of suture-based Maxon samples upon degradation, calculated from the pulsed gradient stimulated echo (PGSTE) spectral intensity log–attenuation plots. The samples degraded for 57 and 67 days showed a deviation from simple linear behavior, and the *D* values were estimated by linear regression, according to eq. (3), for the initial slopes of the plots [Fig. 5(a,b)]. Table II shows, for the initial slopes, that the diffusion coefficients increased with increasing immersion time in PBS solutions. This was consistent with the fact that the polymer matrix became more porous as the immersion time proceeded because of the heterolytic breakdown of the Maxon polymer.

**TABLE II**
**Diffusion Coefficients of the Suture-Based Maxon Samples on Degradation**

| Linear regression | Day 67 $D$ ($m^2/s$) | Day 57 $D$ ($m^2/s$) |
|---|---|---|
| Initial portion of the plot | $1 \times 10^{-10}$ | $9 \times 10^{-11}$ |
| Final portion of the plot | $2 \times 10^{-11}$ | $4 \times 10^{-11}$ |

The nonlinearity shown in Figure 5 could be associated with restricted diffusion,[10] which depended on the geometry of the polymer matrix, or with the distribution of the diffusion coefficients of water molecules when penetrating various phases in the polymer matrix, such as amorphous and crystalline phases or voids.[16] The analysis of the log–attenuation curves presented in this article is, therefore, considered to be only semiquantitative.

## SAXS

Figure 6 shows the SAXS profiles of blank suture-based Maxon samples 1.5 mm thick at different degradation times. The figure indicates three trends. First, the peak position, which arose from $d$, moved to higher angles over the first 40 days and then fell back. Second, the intensity of the peaks increased with the degradation time. Third, the intensity at very low angles increased dramatically after 40 days, eventually dominating the peak. Repeats were carried out for the undegraded samples, and samples were degraded over 30 and 62 days to obtain an estimation of the error. The reproducibility of the repeat results was considered satisfactory overall and was better for short degradation times.

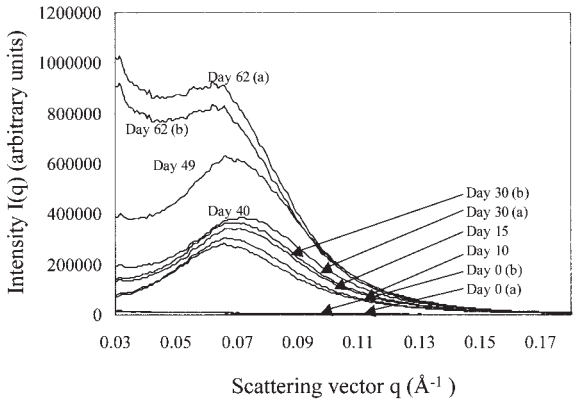


**Figure 6** SAXS profiles of blank suture-based Maxon 1.5 mm thick at different degradation times.

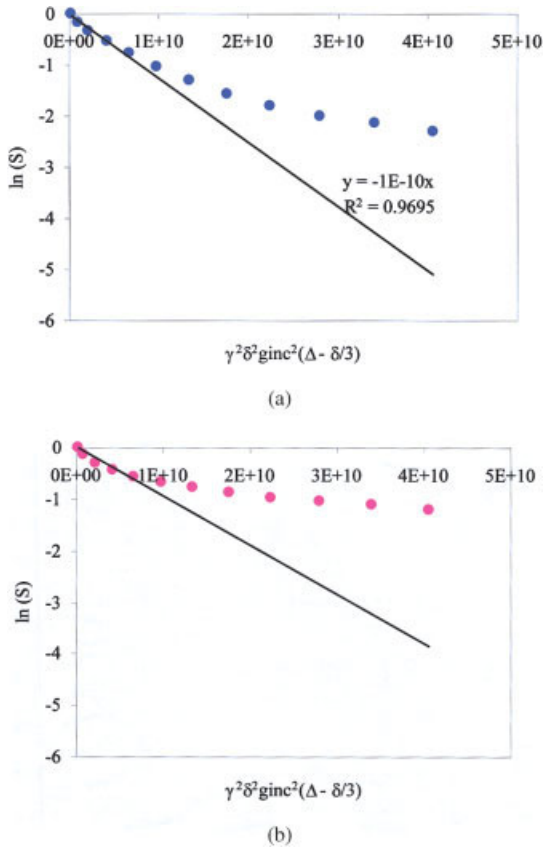


**Figure 5** PGSTE log–attenuation data, with linear regression on the initial portion of the plot: (a) day 67 and (b) day 57.

The $d$ values were determined from the Lorentz-corrected SAXS profiles and are shown in Figure 7. $d$ dropped from approximately 83 to 73 Å over the first 40 days and rose slowly thereafter, reaching 81 Å after 60 days.

Figure 8 shows the $Q$ values as a function of the degradation time. There was a sharp increase over the first 10 days, followed by a slower increase in the subsequent days until 40 days, after which it increased steadily again. The increase in $Q$ over the first 40 days could be correlated with the increase in the intensity of the peaks representing $d$ from the semicrystalline mor-

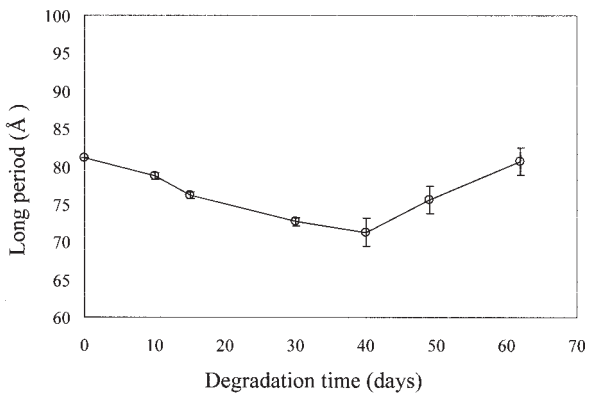


**Figure 7** $D$ of blank suture-based Maxon samples 1.5 mm thick as a function of the degradation time.

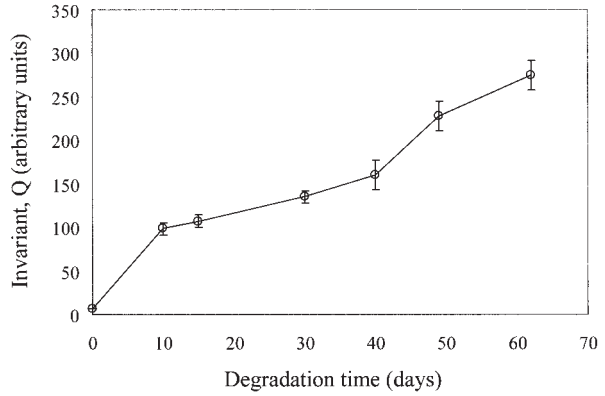


**Figure 8** *Q* of blank suture-based Maxon samples 1.5 mm thick as a function of the degradation time.

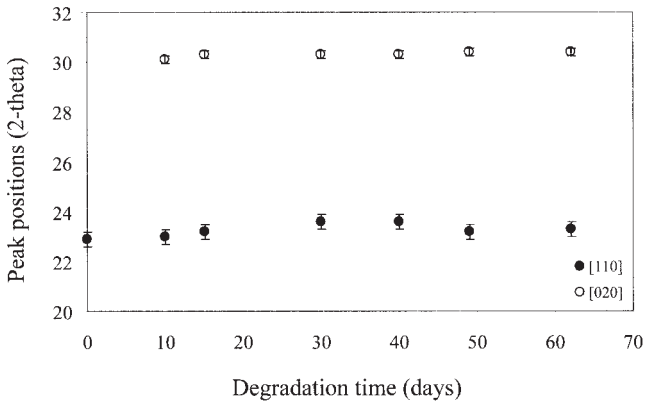


**Figure 10** Changes in the peak positions of (110) and (020) with the degradation time.

phology, as shown in Figure 6. This could be explained by an increase in the crystalline fractions of the polymer, which caused the increase in the electron density difference between the crystalline and amorphous phases. After 40 days, *Q* increased as the intensity increased at lower **q** values, and this was presumably due to the presence of voids created by polymer erosion.

## WAXS

Figure 9 features the WAXS profiles of suture-based Maxon, showing the effect of degradation on the WAXS profiles. These profiles match those of semicrystalline PGA, and it therefore appears that the PGA segments in suture-based Maxon are responsible for the crystalline phase. Two intense peaks, assigned as (110) at $2\theta = 23.3°$ and as (020) at $2\theta = 30.3°$, increased in intensity with the degradation time. The amorphous halo (between $2\theta = 22.6°$ and $2\theta = 38.6°$) decreased significantly in intensity with the degradation time.

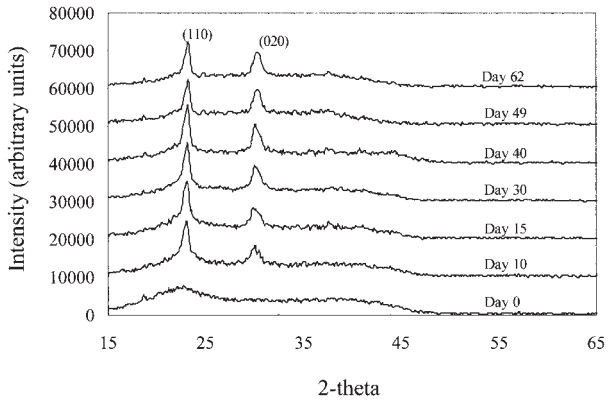


**Figure 9** WAXS profiles of blank suture-based Maxon samples 1.5 mm thick at different degradation times.

The positions of peaks (110) and (020) with the degradation time are plotted in Figure 10. The positions of both peaks were stable during degradation, and this implied that the unit cell of the polymer did not change with time within the experimental error.

The crystallinity percentage was calculated as the area under the crystal peaks divided by the total area under the trace with a cutting-and-weighing technique. Figure 11 shows that the crystallinity increased over the first 40 days, peaking at 35% and remaining relatively constant over longer degradation times. The increase in the crystallinity coincided with the increase in *Q* and the decrease in *d* over the first 40 days. The increase in the crystallinity was likely responsible for the increase in *Q* during this period. As seen for PGA and Maxon B, the mechanism increasing the crystallinity was likely insertion secondary crystallization and the nucleation of new PGA crystals, which explained the reduction in *d*.[7,8,17]

## Thermoporometry

Figure 12 shows thermograms of the heat flow as a function of temperature during the degradation of

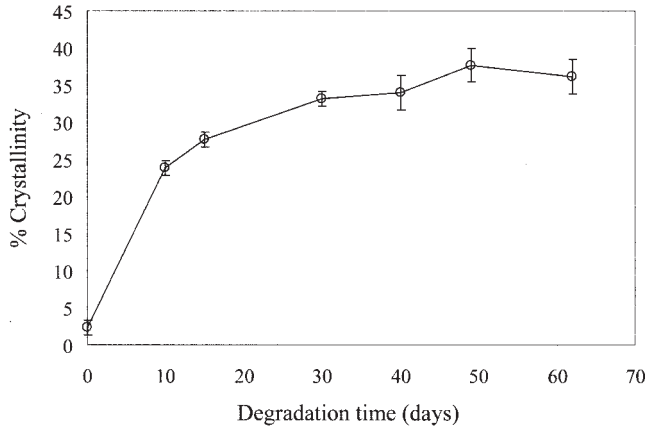


**Figure 11** Crystallinity as a function of the degradation time.

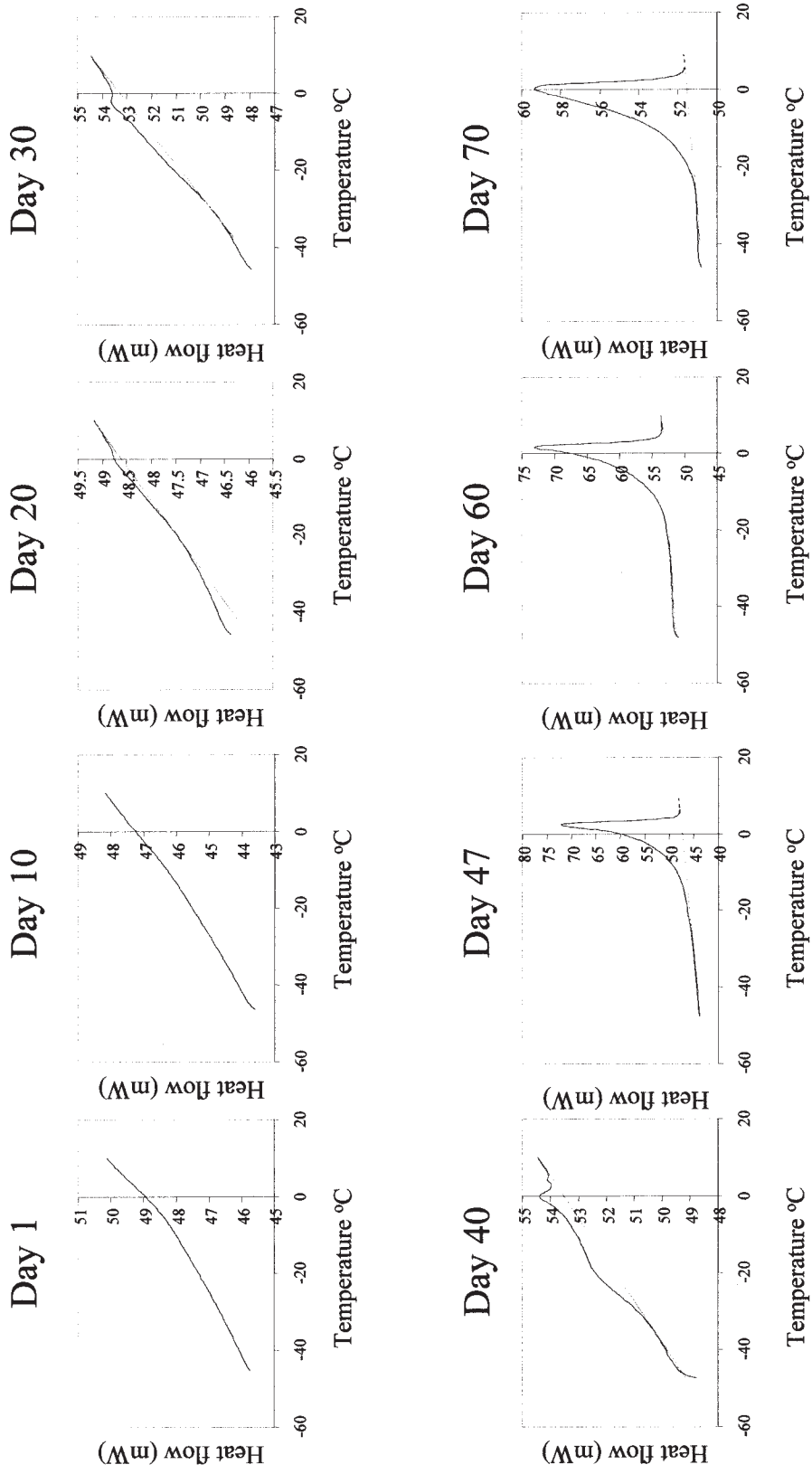


**Figure 12** Differential scanning calorimetry thermograms of the heat flow versus the temperature of blank suture-based Maxon samples 1.5 mm thick at different degradation times. The heating scanning rate was 10°C/min.

**TABLE III**
**$M_w$, $M_n$, and $P_d$ values for Suture-Based Maxon Samples Undegraded and Degraded for 35 Days**

| Sample | $M_w$ (g/mol) | $M_n$ (g/mol) | $P_d$ |
|---|---|---|---|
| Undegraded | 52,450 | 23,850 | 2.20 |
| Day 35 | 6,210 | 3,080 | 2.02 |

blank suture-based Maxon samples 1.5 mm thick. Thermograms taken on day 1 and day 10 showed no peaks for the melting of ice in either the pores or the bulk. This agreed with the low water uptake and mass loss (Fig. 2) and, by implication, the low porosity in the polymer after these degradation times. At 20 and 30 days, the thermograms showed small but significant melting peaks due to the development of small pores. However, the peaks merged, and this made it difficult to determine the pore size distribution during this degradation period.

The thermogram taken on day 40 showed two peaks, which corresponded to the melting of ice in the pores at approximately −20.2°C and the melting of the ice in the bulk around 0.3°C. Both melting peaks appeared inseparable from 47 days onward. Therefore, it was not possible to analyze the peaks for these late degradation times and to determine the pore size distribution.

### GPC

Table III presents the weight-average molecular weight ($M_w$), number-average molecular weight ($M_n$), and polydispersity ($P_d$) data for undegraded and 35-day-degradation suture-based Maxon samples. The results show that $M_w$ of the polymer was reduced significantly over 35 days from 52,450 to 6210 g/mol. The profiles of the water uptake and mass loss (Fig. 2) indicated that significant polymer erosion began at approximately 35 days, the same time point tested with GPC.

### Drug release

Given that the thickness of the samples in this work was carefully controlled, it was possible to plot the absolute amount of the drug released per unit of the surface area of the samples, as shown in Figure 13. Figure 13 shows that the release was little affected by the sample thickness over the first 20 days. Release rates than increased between 20 and 60 days. The thicker samples finished releasing at longer degradation times, but the release profiles between 20 and 60 days did not superimpose on each other. These observations were quite different from those for PGA[9] and Maxon B,[17] for which the superimposition of the release profiles was seen over the entire period of drug release.

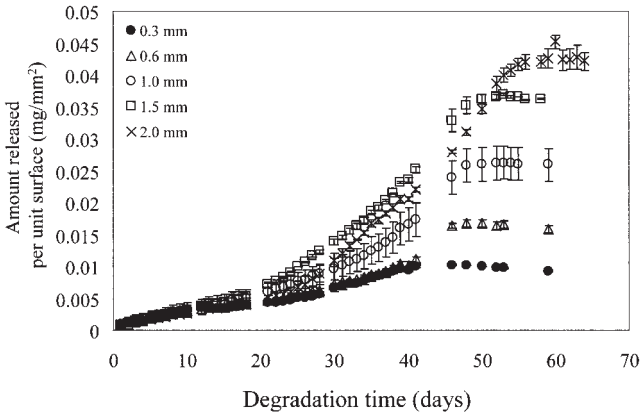


**Figure 13** Cumulative absolute amount of the drug released per unit of the surface area of suture-based Maxon loaded with 5 wt % theophylline in unstirred solutions.

The effect of using different drug systems is shown in Figure 14, in which the absolute amount of the drug released per unit of the surface area for samples containing sulfadiazine is shown. Again, the release rate was slow over the first 20 days and was faster between 20 and 60 days. Between 60 and 100 days, the drug continued to be released very slowly, and the completion of drug release occurred at longer degradation times between 100 and 120 days, as opposed to 60 days for theophylline-loaded samples. The drug-release profiles superimposed on each other but only in the period between 0 and 30 days. This again suggested that the sample thickness did not affect the release rate at short degradation times.

## DISCUSSION

The results presented in this article suggest that, like PGA[9] and Maxon B,[17] suture-based Maxon undergoes

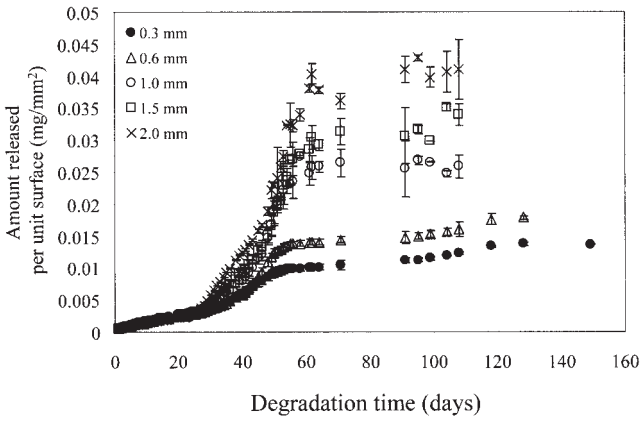


**Figure 14** Cumulative absolute amount of the drug released per unit of the surface area of suture-based Maxon loaded with 5 wt % sulfadiazine in unstirred solutions.

a multistage hydrolytic degradation process. The degradation behaves similarly to that of PGA but occurs over a different timescale. The degradation stages are categorized in order of occurrence into nonactive, active, and postactive stages.

### Nonactive period: Stages 1 and 2

These stages occur over the first 20 days and are characterized by a low level of polymer hydration, after which the water level remains quite constant, low polymer mass loss, and accompanying crystallization of the polymer. Stage 1 may be defined as the initial hydration step, whereas stage 2 begins once the water level stops rising. Five pieces of data support this description of the nonactive period. First, the profiles of the water uptake and mass loss (Fig. 2) reveal very low levels of hydration and negligible mass loss. This is supported by the lack of a water signal detected in the MRI images before 35 days (not shown). Second, the pH of the degradation medium is stable, as shown in Figure 3, and this agrees well with the mass-loss data. Third, the reduction in $d$, the increase in $Q$, and the crystallinity percentage suggest that insertion secondary crystallization and the nucleation of new crystals of PGA are taking place,[7–9] as described for PGA. Fourth, no pores are found with thermoporometry, and this is related to the lack of mass loss and water uptake (Fig. 12). Fifth, the samples turn opaque, and this reflects the increase in the crystallinity, which allows the degraded polymer to scatter light.[18]

During this period, drug release is relatively slow. As the polymer mass loss is negligible and the presence of pores is not detected, the relatively slow drug release observed is likely to be diffusion-controlled and not governed by polymer erosion. The exact rate of drug diffusion will be moderated by plasticization by water and by crystallization. A nonactive stage is also observed for homopolymer PGA, for which it lasts approximately 10 days,[7–9] and for Maxon B, for which it lasts for 20 days.[17] However, in these two polymers, the level of release is much lower in this stage than seen in suture-based Maxon. The drug apparently is more able to diffuse through the preactive matrix of suture-based Maxon than it is through PGA or Maxon B at a similar point of degradation.

### Active period: Stage 3

After about 20 days, an active stage is seen. Changes become particularly marked after about 40 days. The active stage is characterized by significant polymer degradation involving macroscopic and microscopic changes and rapid drug release. Between 20 and 60 days, an increase in the water uptake and mass loss are observed (Fig. 2). A major drop in the degradation medium pH (from 7.4 to 4.5; see Fig. 3) is seen because of the leaching of acidic degradation products. At this stage in the degradation, oligomers become soluble and diffuse into the buffer medium. The molecular weight at 35 days is 6210 g/mol, and this suggests that the critical molecular weight for the solubilization of degradation products is around this value. The sample thickness does not affect the water uptake, mass loss, or pH profiles, within the uncertainties of the measurement technique. $d$ reaches a minimum after 40 days and increases slowly thereafter (Fig. 7). Although insertion secondary crystallization is likely to be responsible for the initial fall in $d$, the subsequent rise may be attributed to swelling within the semicrystalline polymer structure as water is absorbed and oligomers are solubilized (Fig. 2). $Q$ also increase in this period (Fig. 8). Because the crystallinity of the polymer has reached a plateau (Fig. 11) at this point, the increase cannot be explained by changes in the crystalline fraction. The increase in the SAXS signal at very low angles (Fig. 6) suggests the presence of voids within the structure. This is confirmed qualitatively by thermoporometry (Fig. 12). The increase in $Q$ at this stage is therefore likely to be a result of the creation of water-filled voids, whose electron density is much less than that of the swollen polymer phase.

The MRI images show increasing water signals with degradation times between 35 and 60 days (Fig. 4). Incorporating theophylline and stirring the degradation medium apparently promote water uptake in the samples (Fig. 4). There is some evidence that at 60 days water is more concentrated at the sample edges. Unlike the hydration pattern of PGA, which shows distinct water fronts from the MRI images, there are no clearly defined reaction–erosion fronts. This more diffuse behavior of polymer hydration is much more similar to that of Maxon B.[17] The PGSTE NMR reveals that $D$ for samples degraded over 67 days is, as expected, slightly higher than that for a sample degraded over 57 days. This suggests the water mobility in samples degraded for longer time has less restriction, presumably because of a larger amount of polymer removal creating a matrix with higher porosity. An increase in the drug-release rate can be seen after about 20–25 days (Fig. 13). This is similar to the behavior of PGA at the beginning of its active stage. However, the data differ in one important respect. The cumulative release per unit of the surface area plotted for PGA and Maxon B samples of different thicknesses superimposes until the release is finished.[9,17] This is clearly not the case for the suture-based Maxon studied here (Figs. 13 and 14), of which thinner samples release more slowly than thicker ones. The explanation for this is likely to lie in the different release behavior in the earlier, nonactive stage. In PGA and Maxon B, very little drug is released in the nonactive stage, and almost all of the drug release is associated

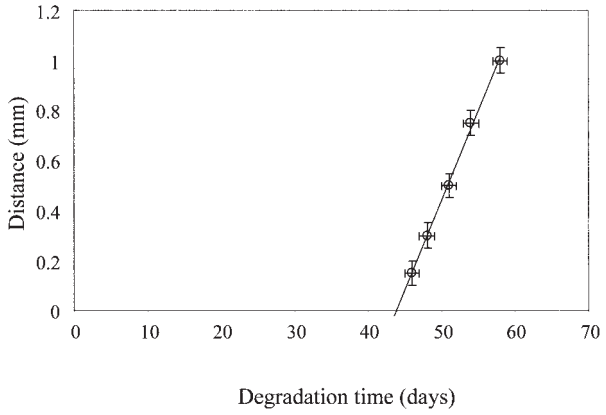


**Figure 15** Plot showing the dependence of the time for complete drug release on the distance moved by reaction–erosion fronts determined from the half-sample thickness of suture-based Maxon samples.

with the increased water uptake and mass loss in the active stage. In contrast, a significant fraction of the drug is released from suture-based Maxon during the nonactive stage. For example, a sample 0.3 mm thick releases nearly 50% before the beginning of the active stage (Fig. 13), as opposed to only 10% for Maxon B[17] and almost 0% for PGA.[9] The mass of the drug released in the preactive stage depends only on the surface available for release and not on the thickness. This means that a larger fraction of the drug is released from thinner samples. The release of such significant proportions of the drug from thin samples in the preactive stage obviously leaves much less for release in the active stage. The distribution of the drug will also be nonhomogeneous. The effect will be a lowering in the rate of release in the active stage that becomes more severe the thinner the sample is.

The release in this case, therefore, seems to be a combination of significant diffusion in the preactive stage and enhanced release controlled by erosion in the active stage. In PGA, the time at which release in this stage finishes is related to the point at which reaction–erosion fronts meet in the center of the sample. The rate of front movement may be inferred from the plotting of the half-thickness of the samples against the time at which release finishes. Figure 15 shows this for suture-based Maxon with the data from the theophylline release in an unstirred solution. If the model is accepted, the intercept of the plot suggests that reaction–erosion fronts start at about 44 days, and the gradient of the plot indicates that the fronts move at a speed of 0.072 mm/day. However, these results must be treated with a degree of caution. It is true that the MRI images show an inhomogeneous distribution of water over the relevant time period. Furthermore, the onset time of the front movement implied by Figure 15 matches well the minimum in $d$, which is related to the point at which swelling starts to dominate the microstructure. On the other hand, significant water uptake can be seen before the implied onset time of 44 days (Fig. 2). The time at which release finishes may be affected by the release that occurring in the preactive stage. Furthermore, as with Maxon B, there is no evidence of the clearly defined reaction–erosion fronts seen in PGA. The water distribution is much more diffuse and is complicated by water-filled fissures and cracks.

In summary, the release of the drug from suture-based Maxon is controlled by diffusion in the early stages and by polymer erosion in the later stages. It differs from that of Maxon B and PGA, in which little diffusion occurs in the preactive stage and release is controlled almost entirely by polymer erosion.

### Postactive stage: Stage 4

After about 60 days, the polymer is very hydrated and porous, and drug release is finished for theophylline. A high level of hydration can be observed from the profiles of the water uptake (Fig. 2) and from the $^1$H MRI images (Fig. 4). The mass loss continues more slowly (Fig. 3). Large cracks appear, and samples eventually fragment into small pieces. The polymer demonstrates a high level of porosity from the thermoporometry study. There is some evidence of a further slow release in samples loaded with sulfadiazine at this point (Fig. 14). This suggests that some of the drug is bound to the polymer and is only freed when these chains are finally released into solution upon degradation. The timeline of the whole degradation and drug-release process is shown in Figure 16.

## CONCLUSIONS

Unoriented suture-based Maxon prepared as discs undergoes a multihydrolysis stage in which four main stages can be identified. The initial nonactive periods (stages 1 and 2) involve very low water uptake and negligible mass loss. Degradation is not accompanied by any appreciable mass loss until a critical molecular weight is reached and the polymer chains are small enough to dissolve into the degradation buffer. Insertion secondary crystallization and the nucleation of new crystals of PGA are also thought to occur during this stage. The drug at this stage releases by diffusion through the polymer matrix. No burst release is observed. The third stage is classified as an active period involving significant rates of water uptake, mass loss, and drug release. Evidence from the mass loss, MRI, thermoporometry, and release profiles suggests that the drug releases through a combination of erosion and diffusion through a porous network that develops as the polymer erodes. There is a dependence on the sample thickness in which thicker samples release for longer degradation times and thinner samples pro-

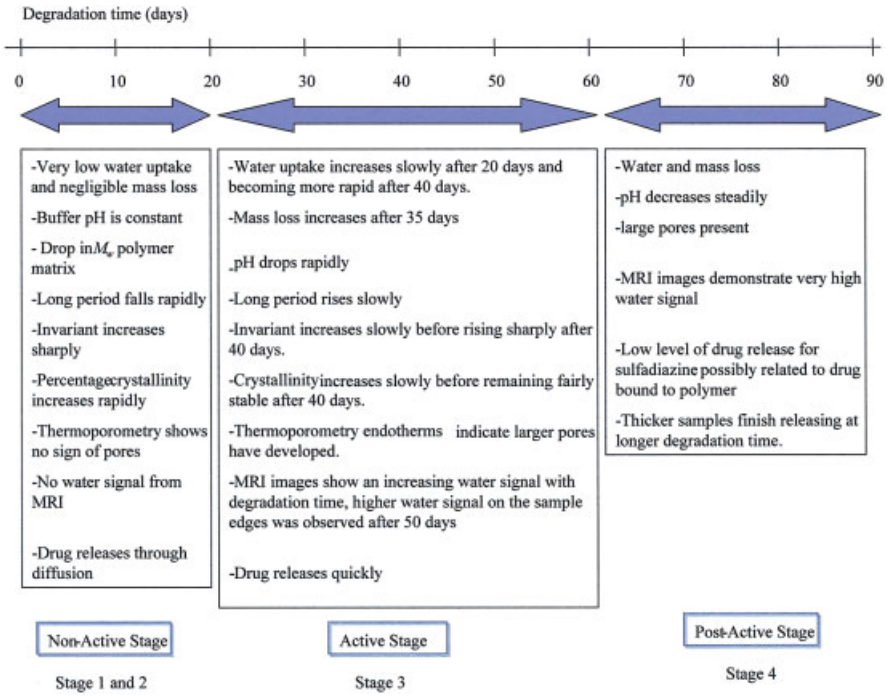


**Figure 16** Timeline summary of the degradation and drug release of suture-based Maxon.

duce slower release rates. The fourth stage, the postactive period, finds the sample in a highly hydrated state containing large cracks. The release of theophylline finishes at this point. Sulfadiazine release continues at a slow rate, in a process that is probably related to the release of the drug bound to the polymer, which is only released when the polymer is solubilized. The release of the drug from suture-based Maxon is therefore controlled by diffusion in the early stages and by polymer erosion in the later stages. It differs from that of Maxon B and PGA, in which little diffusion occurs in the preactive stage and release is controlled almost entirely by polymer erosion.

The authors thank Peter Laity for his experimental assistance with the thermoporometry work. The X-ray experiments were carried out at Daresbury Laboratory with the assistance of Nick Terrill. The authors also thank Georgina Milroy for useful discussions while this article was being prepared.

## References

1. Chu, C. C.; Zhang, L.; Coyne, L. D. J Appl Polym Sci 1995, 56, 1275.
2. Katz, A. R.; Murkherjee, D. P.; Kaganov, A. L.; Gordon, S. Surg Gynecol Obstet 1985, 161, 213.
3. Walton, M. Clin Orthop Rel Res 1989, 242, 303.
4. Metz, S. A.; Chegini, N.; Masterson, B. J. Biomaterials 1990, 2, 41.
5. Casey, D. J.; Roby, M. R. U.S. Pat. 4,052,988 (1984).
6. Chu, C. C. In Wound Closure Biomaterials and Devices; Chu, C. C.; von Fraunhofer, J. A.; Greisler, H. P., Eds.; CRC: Boca Raton, FL, 1997; Chapter 5.
7. Hurrell, S.; Cameron, R. E. J Mater Sci: Mater Med 2001, 12, 811.
8. Hurrell, S.; Cameron, R. E. J Mater Sci: Mater Med 2001, 12, 817.
9. Milroy, G. E.; Cameron, R. E.; Mantle, M. D.; Gladden, L. F.; Huatan, H. J Mater Sci: Mater Med 2003, 14, 465.
10. Callaghan, P. T. Principles of Nuclear Magnetic Resonance Microscopy; Oxford University Press: Oxford, 1991.
11. Harris, R. K. Nuclear Magnetic Resonance Spectroscopy: A Physicochemical View; Longman Scientific & Technical: Essex, England, 1991.
12. Stejskal, E. O.; Tanner, J. E. J Chem Phys 1965, 42, 288.
13. Ryan, A. J.; Nylor, S.; Komanschek, B.; Bras, W.; Mant, G. R.; Derbyshire, G. E. Am Chem Soc Symp 1994, 581, 162.
14. Hay, J. N.; Laity, P. R. Polymer 2000, 42, 6171.
15. Brun, M.; Lallemand, A.; Quinson, J. F.; Eyraud, C. Thermochim Acta 1977, 21, 59.
16. Hollewand, M. P.; Gladden, L. F. Chem Eng Sci 1995, 50, 309.
17. Noorsal, K. Ph.D. Thesis, University of Cambridge, 2003.
18. Young, R. F.; Lovell, P. A. Introduction to Polymers, 2nd ed.; Chapman & Hall: London, 1982.